International Journal of Mathematical, Engineering and Management Sciences
Vol. 9, No. 3, 499-515, 2024
https://doi.org/10.33889/IJMEMS.2024.9.3.026

Ram Arti Publishers

A Novel Approach for Implementing and Optimizing Proportional-Resonant Controller and L-C-L Filter for Single-Phase Grid-tie Inverter

Nibedita Swain
Department of Electrical and Electronics Engineering,
Silicon Institute of Technology, Bhubaneswar, Odisha, India.
E-mail: nswain@silicon.ac.in

Papia Ray
Department of Electrical Engineering,
Veer Surendra Sai University of Technology, Burla, Sambalpur, Odisha, India.
E-mail: papiaray_ee@vssut.ac.in

Majed A. Alotaibi
Department of Electrical Engineering,
College of Engineering, King Saud University, Riyadh, Saudi Arabia.
E-mail: MajedAlotaibi@ksu.edu.sa

Hasmat Malik
Department of Electrical Power Engineering,
Universiti Teknologi Malaysia (UTM), Johor Bahru, Malaysia.
&
Department of Electrical Engineering,
Graphic Era (Deemed to be University), Dehradun, Uttarakhand, India.
E-mail: hasmat.malik@gmail.com

Fausto Pedro García Márquez
Ingenium Research Group,
Universidad Castilla-La Mancha, 13071, Ciudad Real, Spain.
E-mail: faustopedro.garcia@uclm.es

Asyraf Afthanorhan
Universiti Sultan Zainal Abidin (UniSZA),
Gong Badak, Kuala Terengganu, 21300, Terengganu, Malaysia.
E-mail: asyrafafthanorhan@unisza.edu.my

(Received on September 16, 2023; Revised on December 5, 2023 & March 6, 2024; Accepted on March 18, 2024)

Abstract
This article introduces the design procedure of a 1-phase full-bridge inverter for grid-connected applications. The main idea of modelling a full-bridge inverter is that it plays a vital role in solar energy systems. The dynamic equations are formed with the state-space averaging (SSA) technique. A Small-signal averaged model of a full-bridge inverter is constructed by assuming grid current and capacitor voltage as the two states. The voltage and current controller scheme are based on the frequency domain approach. The voltage controller is designed to maintain fixed voltage, and the current controller is used for controlling grid current. The LCL filter is connected to the inverter to provide better harmonic elimination and filter size minimization. This filter is formed by parallel-series combination of inductance and capacitance to improve the overall system performance. Here, a passive damping method is incorporated to make a balanced steady system. Finally, a proportional integral and proportional resonant (PI-PR) controller is introduced to provide better stability and tracking. The detailed analysis of PR controller is explored and demonstrated by MATLAB simulation.

Keywords- 1-phase full bridge inverter, State space averaging technique, LCL filter, Proportional resonant controller, Damping resistor.

1. Introduction

Four IGBT switches and a harmonic (LCL) filter make up the single-phase full-bridge inverter used by grid-connected inverters. The inductance of the harmonics filter lowers current distortion. As a power controller between the grid and the DC link, the inverter must be used (Bose, 2017). To convert DC to 50Hz AC linked to the grid, DC voltage is applied to the inverter. Circuitry for voltage regulation is designed to keep the load side voltage fixed. The PR voltage regulator is used for controlling voltage deviation when voltage signal from the inverter output is compared to the 230 V reference voltage (Mohan et al., 2002). This causes the control block (switch) of the DC/AC inverter to be opened and closed using PWM modulation (Liserre et al., 2005).

For a grid-tied inverter, an LCL filter is often chosen to eliminate switching harmonics. In this paper, LCL parameters such as inverter part inductance (L_i), grid face inductance (L_g), filter capacitance (C) along with damped resistor (R_d), & capacitor current feedback were discussed. The purpose behind the LCL filter is to improve quality of current. Hence suitable values of inverter-side inductance & filter capacitance is needed to limit inverter-side current & rectify low-order current harmonics (Renzhong et al., 2013). The overall objectives of this paper are mentioned below:

- First, the LCL filter is designed to mitigate the harmonics at the grid end to reduce unexpected resonance and make the system more efficient.
- Introducing an LCL filter causes instability due to its inherent resonant frequency, and therefore it requires some sort of damping. Secondly, the damping resistor value should be properly calculated to suppress harmonic losses caused by LCL filter.
- Third, the inverter transfer function is determined using averaging technique to check the stability.
- Accurate K_p and K_i values are calculated for proportional resonant voltage and current controller.

The PR controller is presented in the paper to regulate grid voltage and current. (Reznik et al., 2014). Along with the PR controllers (Ghoshal and John, 2015; Teodorescu et al., 2006) harmonic compensator is incorporated to compensate for the lower-order harmonics which is not required in the system. The proposed structure of grid tie inverter along with LCL filter and PR controller is illustrated in Figure 1. The loads are AC loads. The output of the AC load is matched with the reference voltage and the error is passed through the PR controller to establish a small current. This current is added to the load current to produce the reference inverter current. This reference inverter current is compared with the output of the inverter current and the difference in error is passed through the PR current controller to produce line voltage. This voltage is added to the load voltage to produce the reference voltage. The reference voltage is matched with the carrier voltage to produce gate pulse which is provided to the inverter switch.

The organization of paper is as follows: In section 2 all the components of LCL filter are designed based on some assumptions and the transfer function is obtained without and with using damping resistor. In section 3 two controllers, voltage controller and current controllers are described and K_p, K_i values are formulated. In section 4 grid-tied single phase inverter is proposed and the mathematical equations are derived for different switching states. The state space representation is also discussed. In section 5 all the MATLAB models and the results are depicted.

The main idea behind this paper is to introduce a PR controller that provides high gain at fundamental frequency and accomplishes no steady-state error. PR controller comes under a linear controller using PWM technique. Various current controlled methods for grid tie inverters are PI controller, PR controller, proportional deadbeat and repetitive controller. PR filters produce reference harmonic command precisely in an active power filter, especially for single-phase systems, where *d–q* transformation theory is not directly applicable.

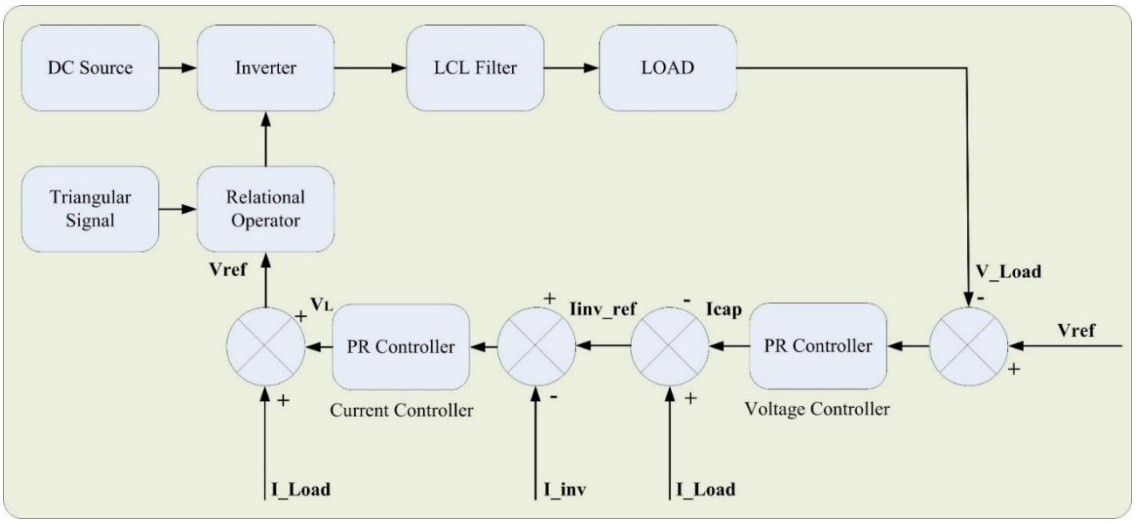

Figure 1. Proposed model of grid-tied inverter.

2. Brief Detail of LCL Filter and Design Consideration

The filter is introduced in grid-connected inverter to reduce the disturbances present at the output side. Different types of filters are used on a large grid side. They can reduce power loss and high attenuation performance. The parameters selection process of LCL filter is studied by (Akagi, 2005; Liserre et al., 2005; Zmood et al., 2001). The capacitance of the LCL filter is calculated by considering 5% of the total power stored. The empirical formula used to determine the capacitance is given in Equation (1).

$$C = \frac{5\,\%\,of\,S}{2\pi f {V_g}^2} \tag{1}$$

In the above expression *'S'* represents the apparent power, *C* is the filter capacitance present in the shunt branch, *'f'* is the supply frequency (50 Hz) and *'V_g'* represents the grid side voltage. The inverter part inductor design is based on a large permissible current ripple. It is assumed to be 20% for this system. The formula is given in Equation (2).

$$L_i = \frac{V_{dc}}{4 f_{sw} \Delta I_{pmax}} \tag{2}$$

V_{dc}, f_{sw}, and I_{pmax} represent the input voltage to the inverter, switching frequency of the inverter, and maximum current ripple respectively. The grid end inductance is measured by the formula specified in Equation (3).

$$L_g = \frac{10\,\%\,of\,V_g}{2\pi f(\frac{S}{V_g})} - L_i \tag{3}$$

L_g and L_i are the filter inductance at the grid end and filter inductance at the inverter end respectively. These are present in the series branch.

The frequency of resonance of LCL filter is obtained using relation Equation (4).

$$\omega_{res} = \sqrt{\frac{L_g+L_i}{L_g L_i C}} \tag{4}$$

The apparent power and the resonant frequency are 2 kVA and 1239 Hz respectively.

By using the values of V_{dc}=400 Volt, V_g=230 Volt, f=50 Hz, P_{out}=2 kVA, f_{sw}=10 kHz, and ΔI_{pmax}, the values of L_i, L_g, and C are obtained as 4.06 mH, 8.41mH and 6.01µF respectively. A Damping resistance (R_d) is connected in series with capacitor C to enhance stability and reduce resonance (Wessels et al., 2008; IEEESTD, 2014). This is termed passive damping. The LCL filter configuration with damping resistor in a shunt branch is depicted in Figure 2.

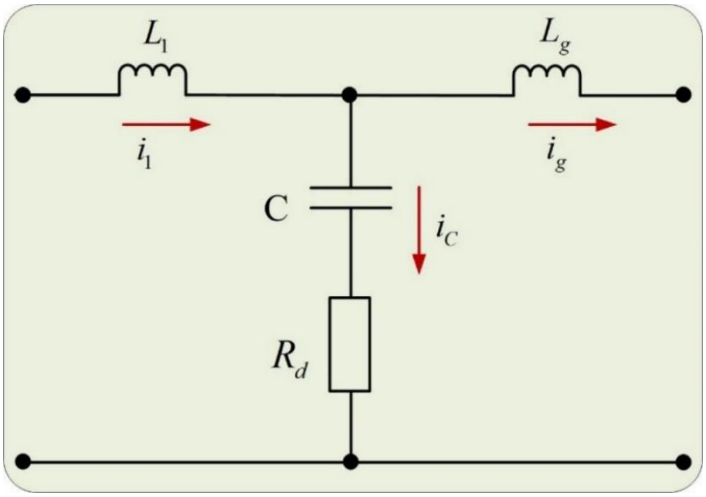

Figure 2. LCL filter configuration.

The damping resistor value should be much lower than the value of the filter capacitive reactance at switching frequency i.e. R_d<X_c at frequency f_{sw}.

The output-to-input ratio of LCL filter without considering damping resistance R_d is illustrated in Equation (5). Inverter current is considered as output and inverter voltage is considered as input (Büyük et al., 2015; Castill et al., 2008).

$$\frac{I_i(s)}{V_i(s)} = \frac{1+L_g C s^2}{L_g L_i C s^3+(L_g+L_i)s} \tag{5}$$

By putting the filter parameters value in Equation (5), the transfer function is obtained as in Equation (6).

$$\frac{I_i(s)}{V_i(s)} = \frac{1+2.614\times10^{-8}s^2}{1.061\times10^{-10}s^3+0.00841s} \tag{6}$$

When the damping resistor R_d is considered, the transfer function of the LCL filter is

$$\frac{I_i(s)}{V_i(s)} = \frac{1+L_gCs^2+R_dCs}{L_gL_iCs^3+(L_gR_dC+L_iR_dC)s^2+(L_g+L_i)s} \quad (7)$$

By putting L_i, L_g, R_d, and C values in Equation (7), the filter transfer function is obtained as in Equation (8).

$$G_f(s) = \frac{2.614\times10^{-8}s^2+2.524\times10^{-8}s+1}{1.061\times10^{-10}s^3+2.123\times10^{-10}s^2+0.00841s} \quad (8)$$

By adding a damping resistance in series with the capacitance, the amplitude at the resonant frequency is reduced and another pole is added in the negative half of s-plane. Hence it increases stability. The resonant peak value is 105 dB at resonant frequency when the damping resistance is not added and its value is reduced to 33.5 dB by adding a damping resistance.

3. Design of Controller

In this work, two controllers are used. One PR controller is employed for controlling the voltage and another PR controller is used for controlling the current (Urtasun and Lu, 2015). The voltage controller regulates the voltage and generates the pulse signal for controlling the switches (Raoufi and Lamchich, 2004). The PR current controller achieves high gain at grid frequency & reduces the steady-state error.

3.1 Voltage Controller

The voltage controller keeps the voltage fixed at a specific value to minimize the error irrespective of input side voltage and load conditions. The design method uses classical PI controller since it produces better results while regulating DC quantities (Ayachit et al., 2015).

Calculation of Proportional gain (k_p) Value

It is operating with a frequency of 5 kHz.
Controller time constant (T_c): 200 µs,
C= 6.01 µF (calculated in section 2),
R_c= 0.0042 Ω (assumed very low value of resistance),
K_p= C/T_c=0.03005.

3.2 Current Controller

The overall performance of system is calculated by utilizing Current controller which is employed to control AC-measures (Mahdavi et al., 1997).

Calculation of Proportional gain (k_p) Value

Controller time constant (T_c): 150 µs,
L_i=4.06 mH (Calculated in section 2),
R_{Li}=0.001 Ω,
K_p= L_i/T_c=27.066.

Calculation of Integral gain (k_i) Value

$$G_n = \frac{k_i\omega_r}{\omega_r{}^2-\omega^2} \quad (9)$$

k_i is 100 for voltage controller and 400 for current controller. G_n=0.1. The current controller TF is

$$G_{PR}(s) = k_p + k_i\frac{s}{s^2+\omega_r{}^2} \quad (10)$$

ω_r is the frequency of resonance in radians/second.

Due to the infinite gain of an ideal PR controller, it results in instability. This drawback is eliminated by utilizing a non-ideal PR controller as shown in Equation (11) (Su et al., 2002; Zhang et al., 2006).

$$G_{PR}(s) = k_p + k_i \frac{2\omega_c s}{s^2 + 2\omega_c s + \omega_r{}^2} \quad (11)$$

With Equation (11), the PR controller gain is finite at the resonant frequency. This property of the controller is more feasible in digital systems (Hegazy et al., 2012). The schematic layout of ideal PR controller is depicted in Figure 3.

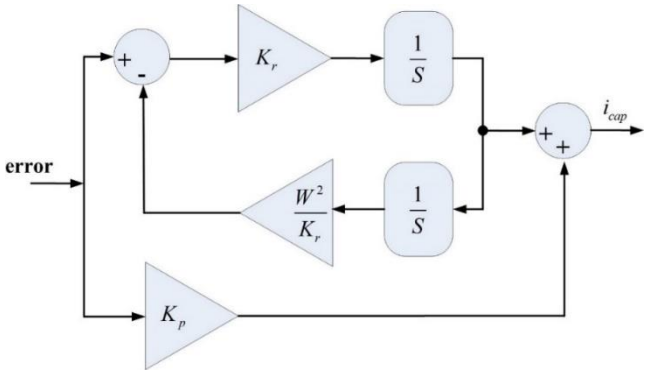

Figure 3. Block diagram of ideal PR controller.

4. Mathematical Modelling of Grid-Connected Inverter

To obtain averaged model for a grid-coupled inverter, certain assumptions are to be taken (Cha and Lee, 2008; Kjaer et al., 2005). First one is that all of the switches are considered to be ideal switches and second one is power the factor should be unity. The mathematical model of the inverter is carried out using SSA technique (Xiaoqiang et al., 2006). Among these four switches, one switch is to be considered as the control switch whose duty cycle is to be controlled by PWM technique (Nordin and Omar, 2011; Swain et al., 2016).

V_g is grid voltage. Inductor L_g & capacitor C are used as energy-storing elements. R_{lg} represents effective series resistance of the inductor. Figure 4 depicts the circuit configuration of 1-phase full-bridge inverter. In this circuit, the electronic switches operate in pairs, and in one half-cycle, switches $S1$ and $S4$ are closed, while in the other half-cycle, $S2$ and $S3$ are closed.

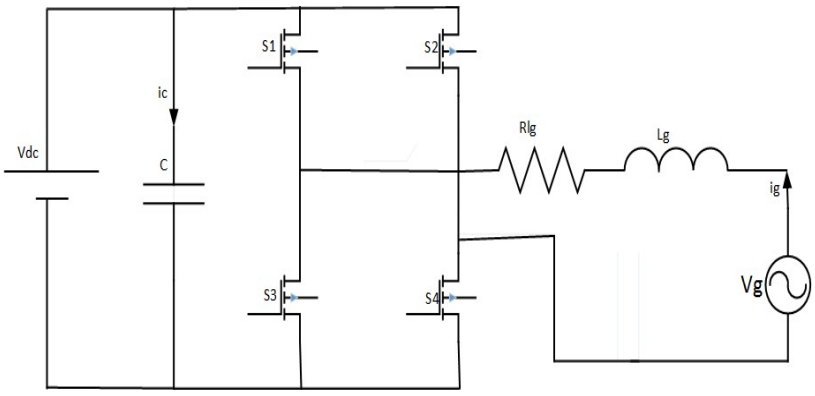

Figure 4. Circuit configuration of 1-phase full-bridge inverter.

Part-A: Switch on State

Figure 5 shows the switch-on state of the inverter circuit. During this state switch *S*3 is on and the current flows from *Vg-Rlg-Lg-S*3-*DS*4-*Vg*. *DS*4 represents the diode of switch *S*4. The on-state equations are formed as follows.

$$L_g \frac{di_g}{dt} = V_g - i_g R_{lg} \tag{12}$$

$$C \frac{dv_c}{dt} = i_c \tag{13}$$

i_g is grid current and v_c is capacitor voltage.

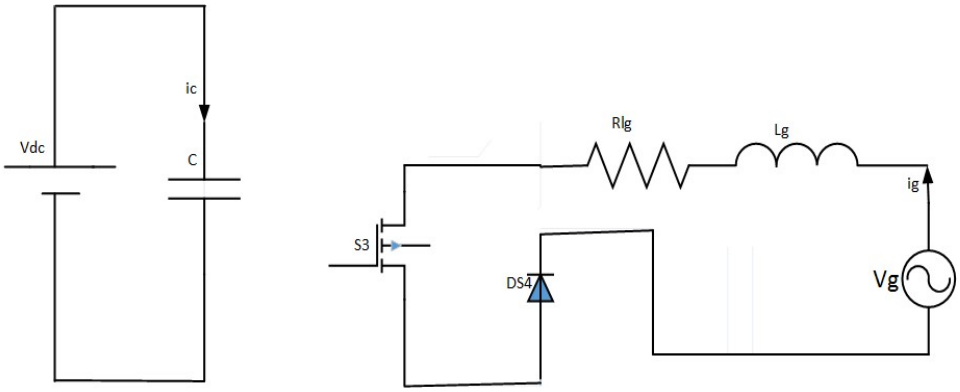

Figure 5. Switch-on state.

Part-B: Switch off State

Figure 6 shows the switch-off state of the inverter circuit. During this state switch, *S*3 is off and the current flows from *Vg-Lg-Rlg-DS*1-*C-DS*4-*Vg*. *DS*1 represents the diode of switch of *S*1. The off-state subinterval equations are formed as follows.

$$L_g \frac{di_g}{dt} = V_g - i_g R_{lg} - v_c \tag{14}$$

$$C \frac{dv_c}{dt} = -i_g \tag{15}$$

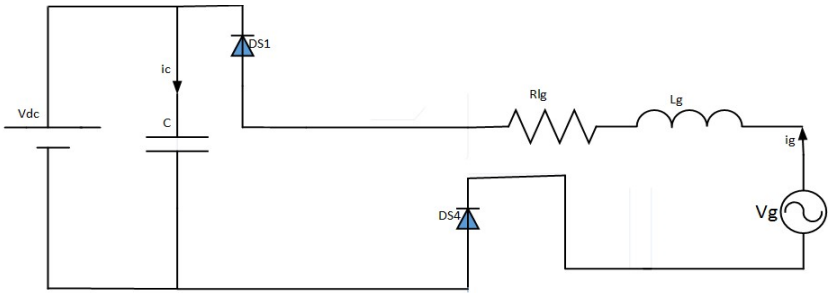

Figure 6. Switch-off state.

The state space form of on-state and off-state matrix is presented in Equation (16) and Equation (17) respectively.

On state matrix form,

$$\begin{bmatrix} \dot{i_g} \\ \dot{v_c} \end{bmatrix} = \begin{bmatrix} -\frac{R_{lg}}{L_g} & 0 \\ 0 & 0 \end{bmatrix} \begin{bmatrix} i_g \\ v_c \end{bmatrix} + \begin{bmatrix} 0 & \frac{1}{L_g} \\ -\frac{1}{C} & 0 \end{bmatrix} \begin{bmatrix} i_c \\ V_g \end{bmatrix} \tag{16}$$

Off-state matrix form,

$$\begin{bmatrix} \dot{i_g} \\ \dot{v_c} \end{bmatrix} = \begin{bmatrix} -\frac{R_{lg}}{L_g} & -\frac{1}{L_g} \\ -\frac{1}{C} & 0 \end{bmatrix} \begin{bmatrix} i_g \\ v_c \end{bmatrix} + \begin{bmatrix} 0 & \frac{1}{L_g} \\ -\frac{1}{C} & 0 \end{bmatrix} \begin{bmatrix} i_c \\ V_g \end{bmatrix} \tag{17}$$

Thus, the state space averaged DC model is represented in Equation (18). '*D*' shows the duty ratio and the value is taken as 0.5.

$$\begin{bmatrix} 0 \\ 0 \end{bmatrix} = \begin{bmatrix} -R_{lg} & -(1-D) \\ -(1-D) & 0 \end{bmatrix} \begin{bmatrix} i_g \\ v_c \end{bmatrix} + \begin{bmatrix} 0 & \frac{1}{L_g} \\ -\frac{1}{C} & 0 \end{bmatrix} \begin{bmatrix} i_c \\ V_g \end{bmatrix} \tag{18}$$

Solving the matrix (18) the state vectors are obtained in Equation (19) and Equation (20).

$$i_g = -\frac{i_c}{(1-D)} \tag{19}$$

$$v_c = \frac{(1-D)V_g + i_c R_{lg}}{(1-D)^2} \tag{20}$$

By applying the perturbation and linearization steps the small-signal control to grid current ratio is stated in Equation (22).

$$G_{inv}(s) = \frac{CV_c s + (1-D)I_g}{CL_g s^2 + CR_{Lg} s + (1-D)^2} \tag{21}$$

$$G_{inv}(s) = \frac{0.2s + 4.345}{2.175\times10^{-6} s^2 + 5\times10^{-7} s + 0.25} \tag{22}$$

5. Simulation Results Demonstration

The results are validated in MATLAB/Simulink platform. Figure 7 shows the frequency response plot of *1*-phase full bridge inverter.

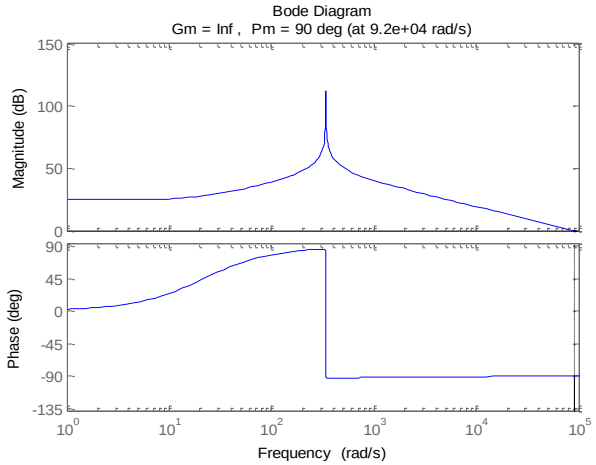

Figure 7. Bode plot of 1-phase full bridge inverter.

From the above plot 7, it is noted that the system is stable with gain margin and phase margin both '+'ve and gain crossover frequency<phase crossover frequency. Figure 8 depicts the bode diagram of LCL filter along with the damping resistance.

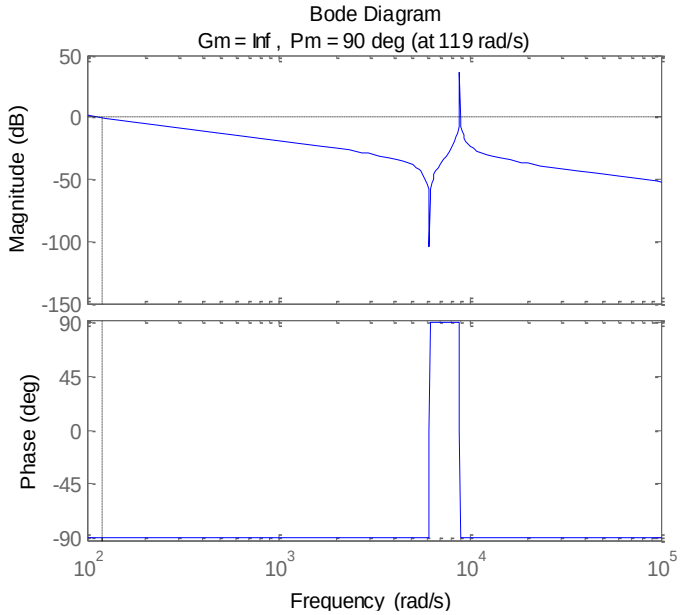

Figure 8. Bode figure LCL filter including damping resistance.

By introducing the damping resistance, the cross-over frequency was reduced to 119 radian/second and also the above plot is a stable one with high gain margin and phase margin. Figure 9 shows bode diagram of cascade combination of filter and inverter.

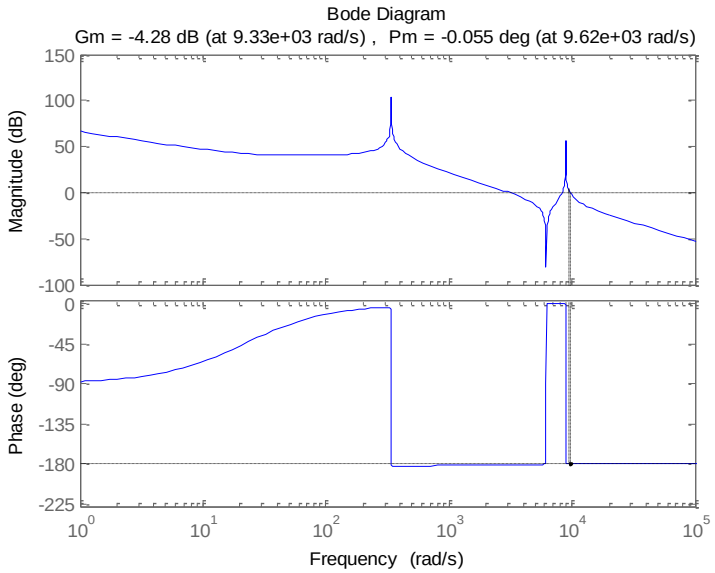

Figure 9. Bode plot of cascade connection of filter and inverter.

By connecting filter along with the inverter, the system goes towards instability. Gain crossover frequency is more than a phase cross-over frequency and has negative gain margin and phase margin. It is purely an unstable system. Figure 10 illustrates root locus plot of the inverter with a PR controller.

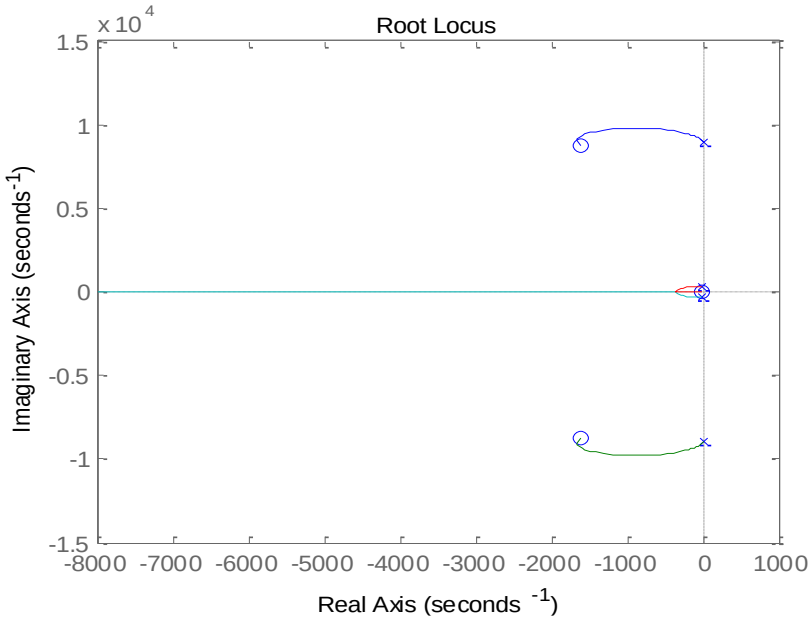

Figure 10. Root locus of the inverter with the PR controller.

From Figure 10, it is observed that the plot is completely lying on the left half of the $j\omega$ axis, hence a stable system. All the pole locations are negative. Figures 11 and 12 show the frequency response plot including both magnitude and phase angle for open-loop and closed-loop systems respectively.

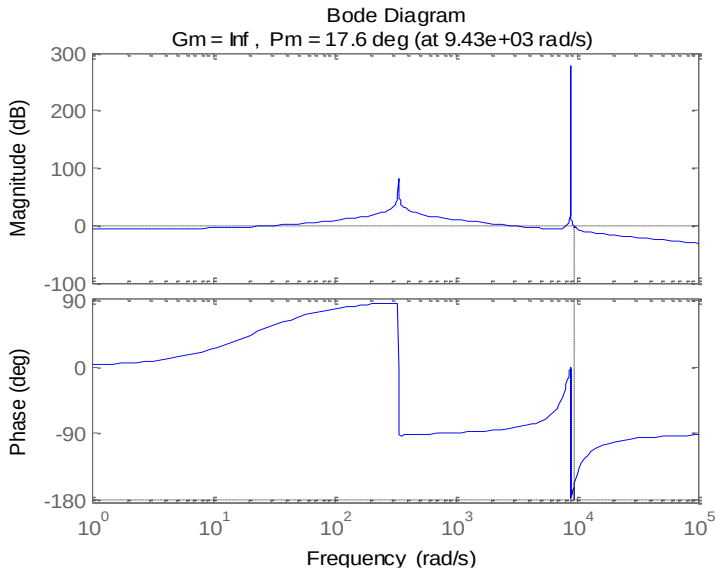

Figure 11. Bode diagram with PR control.

Figure 11 gives the phase margin of 17.6 degrees at a frequency of 9430 radian/second. Hence phase margin has been be improved from 17.6 degrees to a certain margin between 40-60 degrees.

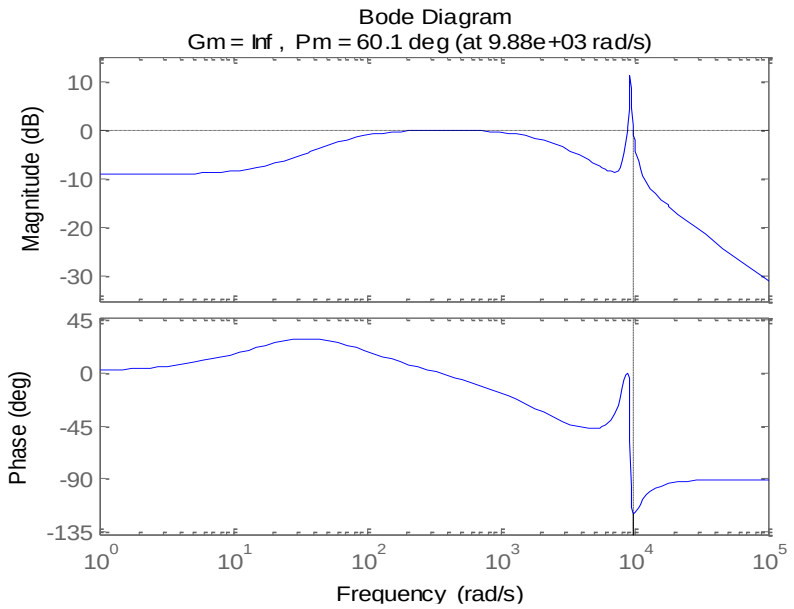

Figure 12. Closed loop Bode diagram with PR control.

From the above Figure 12, the phase margin is 60.1 degrees at 9880 radians/second. The phase margin is improved from 17.6 degrees to 60.1 degrees which is the acceptable one. Figure 13 shows the current waveform of an inverter.

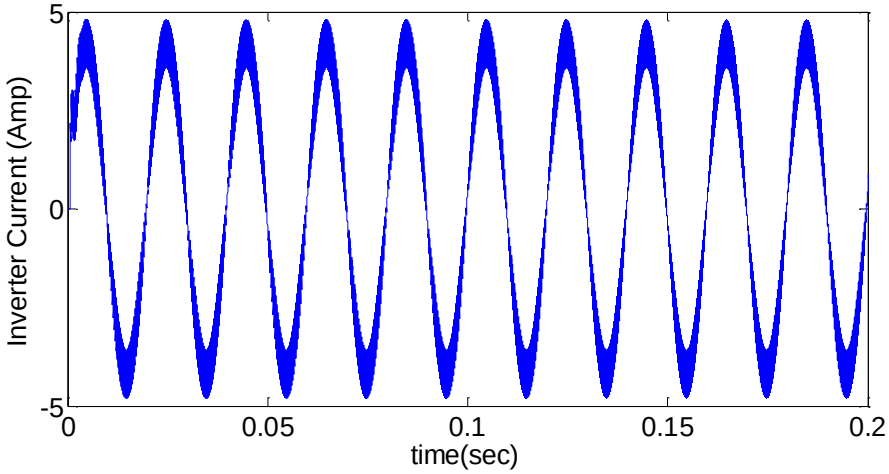

Figure 13. Inverter current waveform.

It is not a smooth sinusoidal current. To make it a pure sinusoidal one, the proper values of *L* and *C* must be chosen for the filter circuit. Figure 14 shows the load current waveform after connecting the filter circuit.

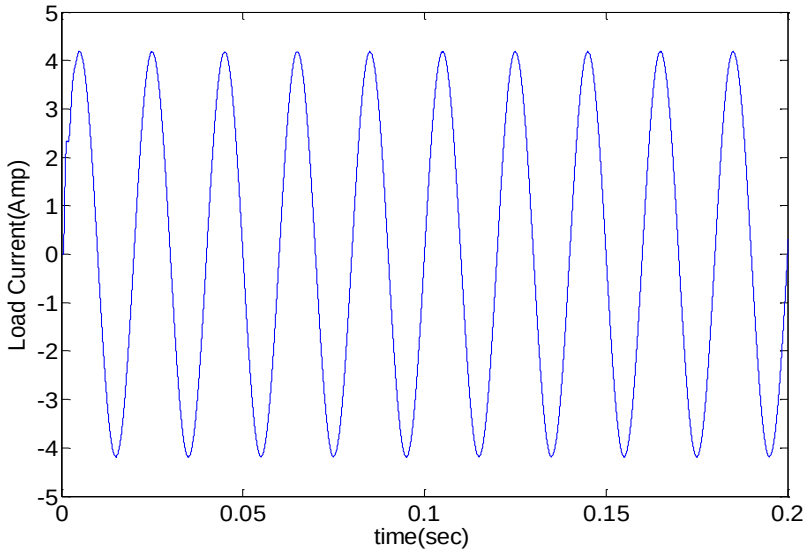

Figure 14. Load current waveform.

It is a smooth sinusoidal current of peak-to-peak magnitude of nearly 8.2 amperes. Figure 15 shows the output voltage across the resistive load.

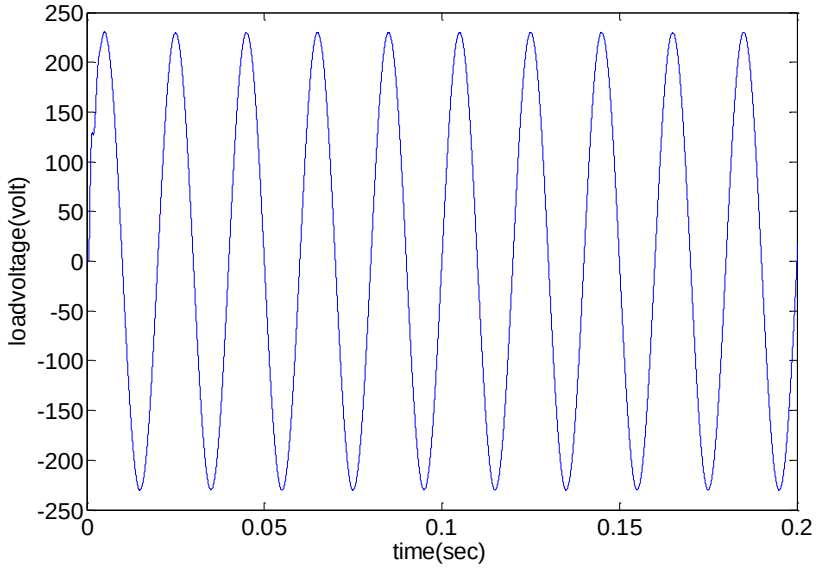

Figure 15. Load voltage waveform.

The output voltage waveform is purely sinusoidal with magnitude of nearly 230 V and it is smooth. Figure 16 shows the load current for different values of load resistance.

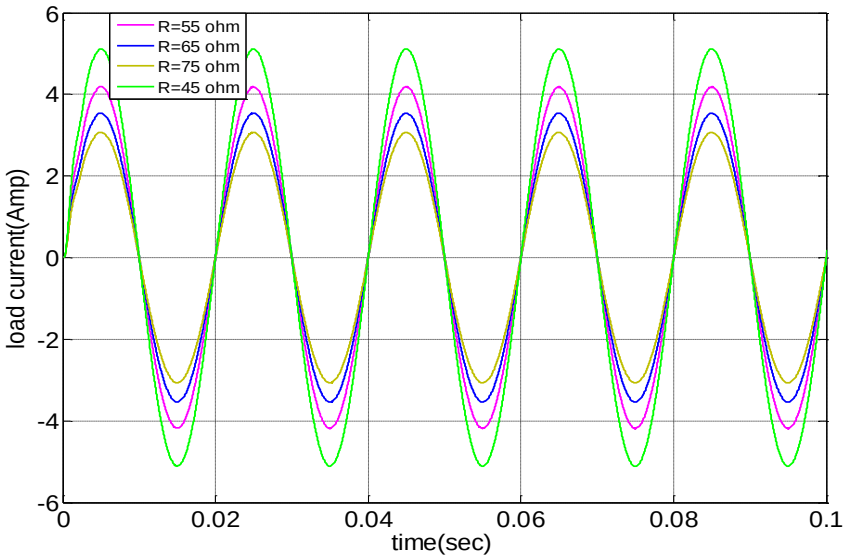

Figure 16. Load current for different load resistance.

It is noticed that the load current is reduced with an increase in value of resistance. It produces smooth sinusoidal currents of different amplitude. Figure 17 illustrates the inverter current waveform for an RL load.

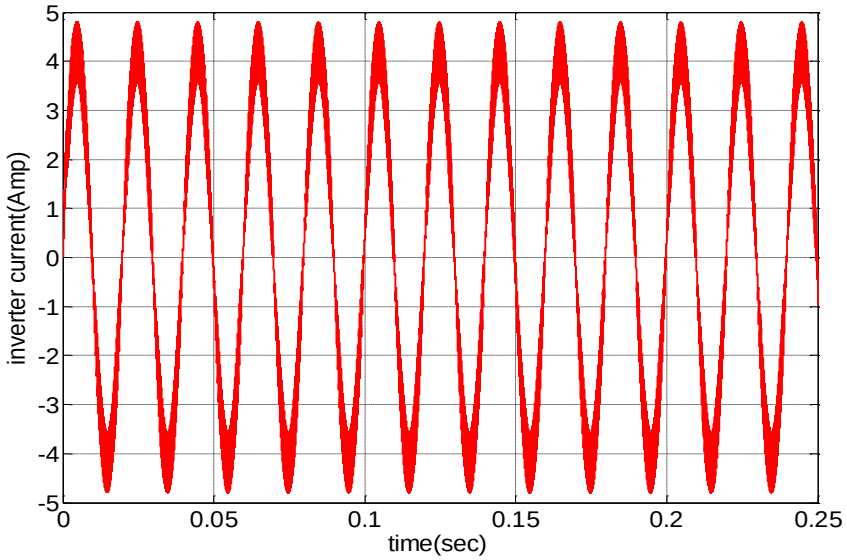

Figure 17. Inverter current for RL load.

The current response is sinusoidal with lot of disturbances. This can be reduced by choosing the right values of *L* and *C* of an LCL filter. Figure 18 shows the inverter current and load current graph for the RL load.

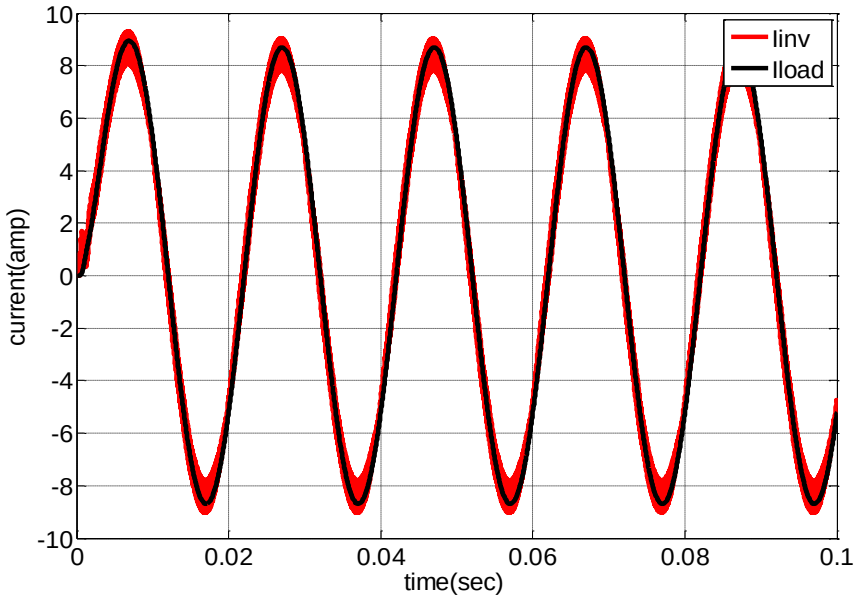

Figure 18. Overlapping of inverter current and load current.

Both the current waveforms have an equal magnitude of 8.6 Amp but the load current waveform is purely sinusoidal. The total harmonic distortion without connecting LCL filter at the grid side is depicted in Figure 19.

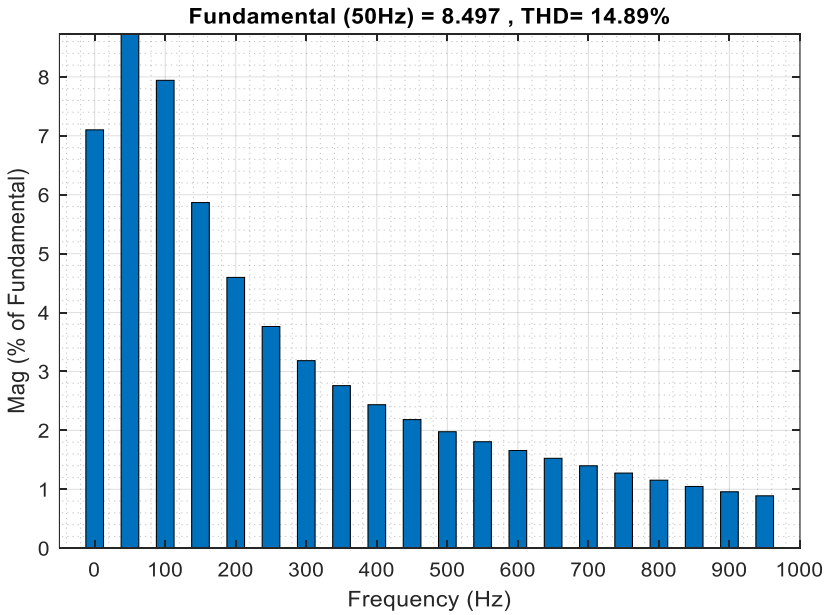

Figure 19. THD without connecting LCL filter.

It is around 15%. By using an LCL filter the THD is not reduced much lower value but the system output is steady without any transients. The THD by using an LCL filter is depicted in Figure 20.

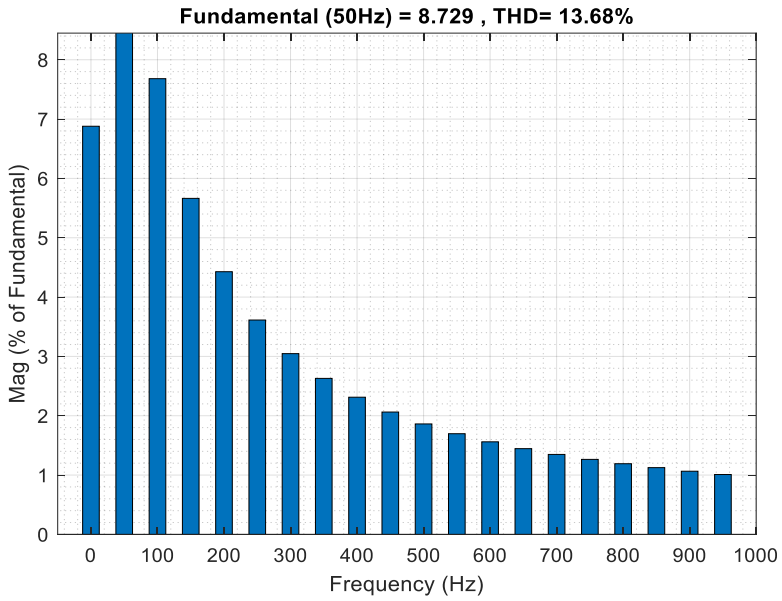

Figure 20. THD with LCL filter.

It is observed that the THD value is 13.68%. By using a harmonic compensator, it can be reduced to a lower value. This paper focuses mainly on the stability of the overall closed-loop system. Table 1 shows the comparison between the open-loop and closed-loop systems.

Table 1. Comparison between open loop and closed loop system.

	Gain crossover frequency(rad/sec)	Phase Margin (Degree)	Phase crossover frequency(rad/sec)	Gain Margin (dB)	Stability
Open loop	9620	-0.055	9330	-4.28	unstable
Closed loop with PR control	9880	60.1	infinite	Infinite	stable

By incorporating PR controller, the phase margin is adjusted to the marginal range and the system becomes a stable one.

6. Conclusion and Future Scope

The 1-Φ grid side inverter is modelled and the dynamic equations are demonstrated and derived by an averaging technique. The control parameters are validated and approximated in frequency domain stability by using methods such as a Bode plot. The inside current controller and outside DC-link voltage controller are properly designed. Through the simulation technique, the controller parameters are properly chosen for regulating the output, irrespective of the load variation. All the simulated results are demonstrated in a step-wise-step manner. Instead of using DC voltage renewable sources like PV can be used. Though the output of PV is not very high, so to get a voltage of 400 volts at the input side a high gain converter can be used. An LCL filter is one of the harmonic compensators that create a low-impedance path for harmonic currents

to flow. The whole system can be modified by using another harmonic compensator like active filter or hybrid filter. The purpose of using two PR controllers is to control both voltage and current and also provide an infinite gain at the fundamental frequency of the AC source. The stability is also improved by adding the damping resistance.

Conflicts of Interest

The authors declare no conflicts of interest regarding this article.

Acknowledgments

The authors extend their appreciation to the Researchers Supporting Project at King Saud University, Riyadh, Saudi Arabia, for funding this research work through the project number RSP2023R278. The authors extend their appreciation to the Researchers Supporting Project at Universiti Teknologi Malaysia (UTM), Malaysia (project no. UTMFR: Q.J130000.3823.23H05). The authors extend their appreciation to Intelligent Prognostic Private Limited Delhi, India; Veer Surendra Sai University of Technology, Burla, Sambalpur, Odisha, India; Silicon Institute of Technology, Bhubaneswar, Odisha, India; Universiti Sultan Zainal Abidin (UniSZA) Malaysia and Ingenium Research Group, Universidad Castilla-La Mancha, 13071 Ciudad Real, Spain for providing technical support in this research work. **For the correspondence**, please contact the corresponding author(s) at MajedAlotaibi@ksu.edu.sa (Majed A. Alotaibi), hasmat@utm.my (Hasmat Malik), asyrafafthanorhan@unisza.edu.my (Asyraf Afthanorhan).

References

Akagi, H. (2005). Active harmonic filters. *Proceedings of the IEEE*, *93*(12), 2128-2141. https://doi.org/10.1109/jproc.2005.859603.

Ayachit, A., Reatti, A., & Kazimierczuk, M.K. (2015). Small-signal modelling of the PWM boost DC-DC converter at boundary-conduction mode by circuit averaging technique. In *2015 IEEE International Symposium on Circuits and Systems* (pp. 229-232). IEEE. Lisbon, Portugal. https://doi.org/10.1109/iscas.2015.7168612.

Bose, B.K. (2017). Power electronics, smart grid and renewable energy systems. *Proceedings of the IEEE Power Electronics*, *105*(11), 2007-2010. https://doi.org/10.1109/jproc.2017.2745621.

Büyük, M., Tan, A., Bayindir, K.C., & Tümay, M. (2015). Analysis and comparison of passive damping methods for shunt active power filter with output LCL filter. In *2015 International Aegean Conference on Electrical Machines and Power Electronics* (pp. 434-440). IEEE. Side, Turkey. https://doi.org/10.1109/optim.2015.7426745.

Castilla, M., Miret, J., Matas, J., De Vicua, L.G., & Guerrero, J.M. (2008). Linear current control scheme with series resonant harmonic compensator for single-phase grid-connected photovoltaic inverters. *IEEE Transactions on Industrial Electronics*, *55*(7), 2724-2733. https://doi.org/10.1109/tie.2008.920585.

Cha, H., & Lee, S. (2008). Design and implementation of photovoltaic power conditioning system using a current based maximum power point tracking. In *2008 IEEE Industry Application Society Annual Meeting* (pp. 1-5). IEEE. Edmonton, Canada. https://doi.org/10.1109/08ias.2008.302.

Ghoshal, A., & John, V. (2015). Active damping of LCL filter at low switching to resonance frequency ratio. *IET Power Electronics*, *8*(4), 574-582. https://doi.org/10.1049/iet-pel.2014.0355.

Hegazy, O., Mierlo, J.V., & Lataire, P. (2012). Analysis, modeling and implementation of a multidevice interleved d.c./d.c. converter for fuel cell hybrid electric vehicles. *IEEE Transactions on Power Electronics*, *27*(11), 4445-4458. https://doi.org/10.1109/tpel.2012.2183148.

IEEE Recommended Practice and Requirements for Harmonic Control in Electric Power Systems. IEEESTD.2014. https://doi.org/10.1109/ieeestd.2014.6826459

Kjaer, S.B., Pedersen, J.K., & Blaabjerg, F. (2005). A review of single-phase grid-connected inverters for photovoltaic modules. *IEEE Transactions on Industry Applications*, *41*(5), 1292-1306. https://doi.org/10.1109/tia.2005.853371.

Liserre, M., Blaabjerg, F., & Hansen, S. (2005). Design and control of an LCL filter-based three-phase active rectifier. *IEEE Transactions on Industry Applications*, *41*(5), 1281-1291. https://doi.org/10.1109/tia.2005.853373.

Mahdavi, J., Emadi, A., & Toliyat, H.A. (1997). Application of state space averaging method to sliding mode control of PWM DC/DC converters. In *IAS '97. Conference Record of the 1997 IEEE Industry Applications Conference Thirty-Second IAS Annual Meeting* (pp. 820-827). IEEE. New Orleans, LA, USA. https://doi.org/10.1109/ias.1997.628957.

Mohan, N., Undeland, T.M., & Robbins, W.P. (2002). *Power electronics: Converters, applications, and designs (3rd edition)*. John Wiley & Sons, New Delhi. ISBN: 978-0-471-22693-2.

Nordin, A.H.M., & Omar, A.M. (2011). Modelling and simulation of photovoltaic (PV) array and maximum power point tracker (MPPT) for grid-connected PV system. In *2011 3rd International Symposium & Exhibition in Sustainable Energy & Environment* (pp. 114-119). IEEE. Malacca, Malaysia. https://doi.org/10.1109/isesee.2011.5977080.

Raoufi, M., & Lamchich, M.T. (2004). Average current mode control of a voltage source inverter connected to the grid: Application to different filter cells. *Journal of Electrical Engineering*, *55*(3-4), 77-82.

Renzhong, X., Lie, X., Junjun, Z, & Jie, D. (2013). Design and research on the LCL filter in three-phase PV grid-connected inverters. *International Journal of Computer and Electrical Engineering*, *5*(3), 322-325. https://doi.org/10.7763/ijcee.2013.v5.723.

Reznik, A., Simoes, M.G., Al-Durra, A., & Muyeen, S.M. (2014). LCL filter design and performance analysis for grid-interconnected systems. *IEEE Transactions on Industry Applications*, *50*(2), 1225-1232. https://doi.org/10.1109/tia.2013.2274612.

Su, J.H., Chen, J.J., & Wu, D.S. (2002). Learning feedback controller design of switching converters via MATLAB/SIMULINK. *IEEE Transactions on Education*, *45*(4), 307-315.

Swain, N., Panigrahi, C.K., & Pati, N. (2016). Comparative performance analysis of dc-dc converter using PI controller and fuzzy logic controller. In *2016 IEEE International Conference on Power Electronics, Intelligent Control and Energy Systems* (pp. 1-5). IEEE. Delhi, India. https://doi.org/10.1109/icpeices.2016.7853232.

Teodorescu, R., Blaabjerg, F., Liserre, M., & Loh, P.C. (2006). Proportional- resonant controllers and filters for grid-connected voltage-source converters. *IEE Proceedings - Electric Power Applications*, *153*(5), 750-762.

Urtasun, A., & Lu, D.D.C. (2015). Control of a single-switch two-input buck converter for MPPT of two PV strings. *IEEE Transactions on Industrial Electronics*, *62*(11), 7051-7060. https://doi.org/10.1109/tie.2015.2432097.

Wessels, C., Dannehl, J., & Fuchs, F.W. (2008). Active damping of LCL-filter resonance based on virtual resistor for PWM rectifiers-stability analysis with different filter parameters. In *2008 IEEE Power Electronics Specialists Conference* (pp. 3532-3538). IEEE. Rhodes, Greece. https://doi.org/10.1109/pesc.2008.4592502.

Xiaoqiang, G., Qinglin, Z., & Weiyang, W. (2006). A single-phase grid-connected inverter system with zero steady-state error. *In 2006 CES/IEEE 5th International Power Electronics and Motion Control Conference* (pp. 1-5). IEEE. Shanghai, China. https://doi.org/10.1109/ipemc.2006.4778040.

Zhang, W., Allgower, F., & Liu, T. (2006). Controller parameterization for SISO and MIMO plants with time delay. *Systems and Control Letters*, *55*(10), 794-802. https://doi.org/10.1016/j.sysconle.2006.03.008.

Zmood, D.N., Holmes, D.G., & Bode, G.H. (2001). Frequency domain analysis of three-phase linear current regulators. *IEEE Transactions on Industry Applications*, *37*(2), 601-610. https://doi.org/10.1109/28.913727.